Materials Transactions, Vol. 45, No. 3 (2004) pp. 958 to 963

EXPRESS REGULAR ARTICLE

Effect of ECAP Strain on Deformation Behavior at Low Temperature Superplastic Regime of Ultrafine Grained 5083 Al Alloy Fabricated by ECAP

Kyung-Tae Park[1], Hang-Jae Lee[1,*1], Chong Soo Lee[2], Byung Du Ahn[3,*2], Hyun Soo Cho[3,*2] and Dong Hyuk Shin[3]

[1]*Division of Advanced Materials Science & Engineering, Hanbat National University, Taejon, 305-719, Korea*
[2]*Department of Materials Sciene & Engineering, Pohang University of Science & Technology, Pohang, 790-784, Korea*
[3]*Department of Metallurgy and Materials Science, Hanyang University, Ansan, 425-791, Korea*

A series of tensile testing was carried out on the ultrafine grained 5083 Al alloy, which was fabricated by equal channel angular pressing (ECAP) with different ECAP strains, at low temperature superplastic (LTS) temperature of 548 K. This investigation was aimed at examining the effect of the ECAP strain inducing different microstructure in the alloy on the deformation mechanisms at LTS regime. The most distinguishable microstructural evolution by increasing the ECAP strain from ~4 to ~8 was an increment of a portion of high angle boundaries while the (sub)grain size remained almost unchanged. The sample after 4 passes (a strain of ~4) did not exhibit LTS, but superplastic elongations were obtained in the sample after 8 passes (a strain of ~8). An analysis of the mechanical data in light of the standard deformation mechanisms revealed that deformation of the sample after 4 passes was governed by dislocation climb while grain boundary sliding attributed to LTS of the sample after 8 passes. The difference of the deformation mechanisms in the present case was discussed in terms of the microstructures developed under different ECAP strains.

(Received October 27, 2003; Accepted February 12, 2004)

Keywords: *5083 aluminum alloy, equal channel angular pressing (ECAP), ultrafine grains, deformation behavior, low temperature superplasticity*

1. Introduction

It is known that some bulk ultrafine grained (UFG, the grain sizes of 0.1~0.5 μm) materials fabricated equal channel angular pressing (ECAP) exhibit the superplatic behavior at temperatures much lower than that for conventional micro-grained (the grain sizes of 1~10 μm) superplastic materials.[1–8] So-called low temperature superplasticity (LTS) is primarily associated with a near-equiaxed UFG structure created by ECAP. In addition to a near-equiaxed UFG structure, high angle grain boundaries are another necessary condition to achieve LTS. Grain boundary misorientation in ECAPed materials is greatly influenced by the ECAP strain as well as the ECAP route.[9–12] Therefore, the superplastic properties of ECAPed UFG materials are much dependent on the ECAP conditions. The previous investigations demonstrated that ECAP of 8 passes (equivalent to an effective strain of ~8) with route B_c resulted in an optimum UFG structure showing the maximum elongation,[13] but elongation was drastically reduced under the identical testing conditions when ECAP less than 8 passes was imposed.[8,13] In case of LTS of the ECAPed UFG commercial Al alloys, for instance, elongation over 300% was obtained by 8 passes with route B_c[7,8] while 4 passes with route B_c resulted in elongation of only ~150%.[8] Although it was argued that the drastic decrease of elongation in the latter case was attributed to a lack of development of high angle boundaries enough to exhibit superplasticity,[12,14] the effect of such a difference in the as-ECAPed microstructures on the deformation mechanisms of the ECAPed UFG Al alloys at LTS regime is still unclear. So, in this study, the effect of the ECAP strain on the deformation mechanisms of the ECAPed UFG 5083 Al alloy was investigated by preparing the alloy under the identical ECAP conditions except the ECAP strain and by conducting a series of uniaxial tensile testing at LTS temperature of 548 K.

2. Experimental Procedures

A commercial 5083 Al alloy (Al-4.4Mg-0.7Mn-0.15Cr (in mass%)) was supplied in the form of extruded bar. Before ECAP, the alloy was annealed at 723 K for 1 hr and the linear intercept grain size of the annealed sample was about 200 μm. After machining the cylindrical samples of ϕ 10 mm × 130 mm from the annealed bar, ECAP was carried out on the samples at 473 K by using an ECAP die designed to yield an effective strain of ~1 per pass: the detailed ECAP procedure and facility are described elsewhere.[15,16] During ECAP, the sample was rotated by 90° around its longitudinal axis in the same direction between the passages, *i.e.* route B_c.[17] ECAP was conducted up to 4 or 8 passes (equivalent effective strains of ~4 or ~8, respectively).

For tensile testing, the specimens of 8 mm (gage length) × 4 mm (width) × 2 mm (thickness) were machined from the as-ECAPed bar. Tensile tests were carried out at initial strain rates of 10^{-5}~10^{-2} s^{-1} at 548 K on a universal testing machine operating at a constant crosshead speed. 548 K which is ~0.64 T_m (T_m: an incipient melting temperature of the alloy in Kelvin) was previously reported to be the optimum LTS temperature for the present alloy.[7] All the tests were performed in a three-zone furnace in air and the testing temperature was controlled within ± 3 K.

Microstructures were examined by transmission electron microscopy (TEM, JEOL 2010 with 200 kV). Thin foils for TEM observation were prepared by the twin-jet polishing technique using a mixture of 25% nitric acid and 75%

*1Graduate Student, Hanbat National University
*2Graduate Student, Hanyang University

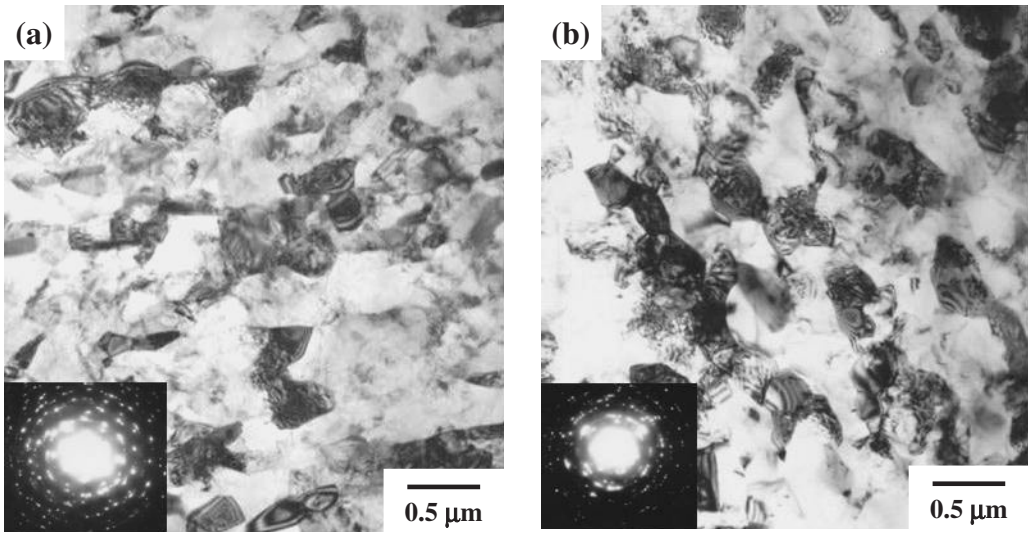

Fig. 1 TEM micrographs of the as-ECAPed 5083 Al alloy (route B_c, 473 K). (a) after 4 passes, (b) after 8 passes.

methanol at an applied potential of 25 V and at 243 K. Boundary misorientation was investigated by a FEG scanning electron microscopy (JSM 6500F) equipped with an electron back-scatter diffraction (EBSD) imaging system (Oxford INCA Crystal). The observation was carried out at least three different area of 12 μm × 12 μm with a beam size of ~37 nm: the beam spot size impinging on the sample surface is slightly larger than the actual beam size.[11] Although the present imaging system can probe below 3° misorientation, the tolerance angle was set to be 3° for the misorientation distribution analysis since uncertainty on the measurement increases below this angle. In addition, the grain structure after failure was observed by optical microscopy (OM) after etching with a dilute Poulton's reagent.

3. Results

3.1 Characteristics of the as-ECAPed microstructure

TEM microstructures of the samples after 4 and 8 passes are compared in Fig. 1. There was no significant difference in the apparent (sub)grain size between the two samples, ~0.3 μm. The general features including ill-defined (sub)-grain boundaries and very high dislocation density were also similar to each other. However, the selected area diffraction pattern of the sample after 8 passes were more diffusive than that after 4 passes, indicating the increment of boundary misorientation with increasing the ECAP strain. The distribution of boundary misorientation of these samples analyzed by EBSD is shown in Fig. 2. In the present case, by increasing the ECAP strain from ~4 to ~8, a portion of boundaries with misorientation less than 10° decreased and that of boundaries with misorientation in the range of 20°~40° increased. But a portion of boundaries with misorientation higher than 40° remained nearly unchanged. Regarding 15° as a critical misorientation between low and high angle boundaries, a portion of high angle boundaries (15°<) increased from ~35% after 4 passes to ~50% after 8 passes. The rate of development of high angle boundaries in the present 5083 Al alloy was much slower than that of pure Al. In case of pure Al, a portion of high angle boundaries reached ~60% after 4 passes and remained almost the same by increasing the ECAP passes.[10,11] Being investigated at present, this could be attributed to weaker texture development and higher discontinuity in the Schmid factor among the operative slip systems in the 5083 Al alloy during ECAP, probably associated with higher ECAP temperature and the presence of alloying elements compared to pure Al: in case of pure Al, ECAP was undertaken at room temperature.

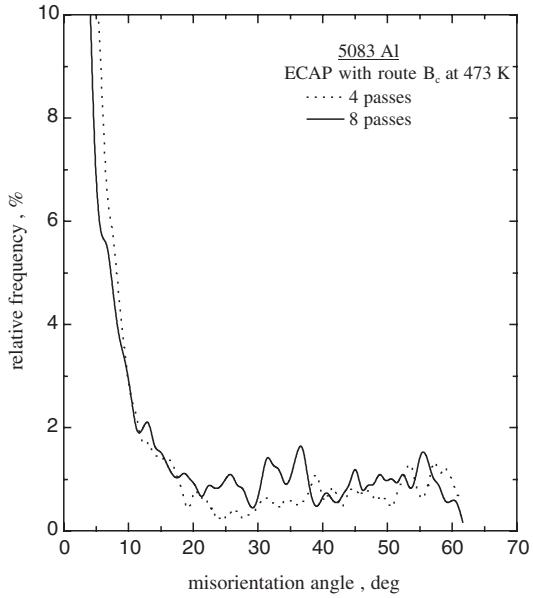

Fig. 2 The distribution of boundary misorientation as a function of misorientation angle for the as-ECAPed 5083 Al alloy (route B_c, 473 K).

3.2 Mechanical data

Figure 3 shows a double logarithmic plot of the maximum true flow stress (σ) against the corresponding true strain rate ($\dot{\varepsilon}$) for the alloy after 4 passes (Fig. 3a) and 8 passes (Fig. 3b). The mechanical data of the alloy after 4 passes were fitted into a straight line with a slope of ~0.2, *i.e.* the strain rate sensitivity m ($= \partial \ln \sigma / \partial \ln \dot{\varepsilon}$) ≈0.2. Contrarily, those of the alloy after 8 passes exhibited the sigmoidal behavior manifested by the presence of the three distinct regions. m

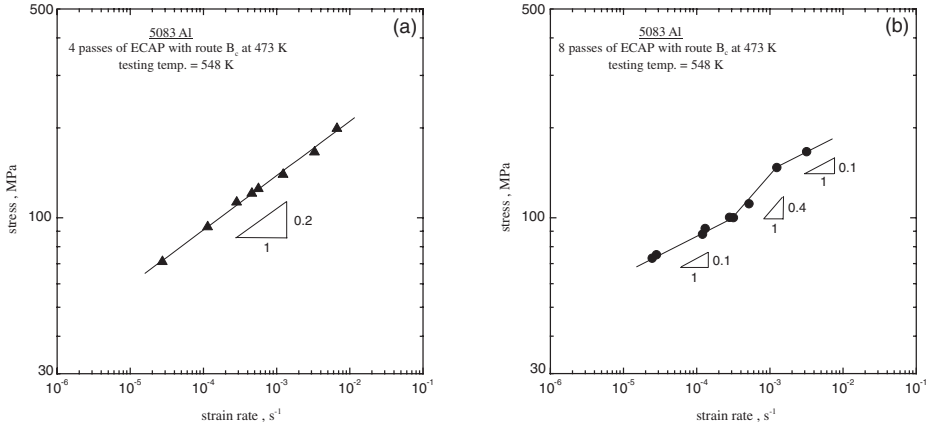

Fig. 3 Maximum flow stress *vs* the corresponding strain rate in a double logarithmic scale for the as-ECAPed 5083 Al alloy (route B_c, 473 K) tested at 548 K. (a) after 4 passes, (b) after 8 passes.

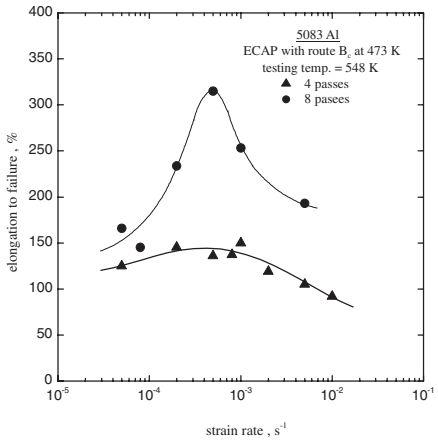

Fig. 4 Variation of elongation to failure as a function of the initial strain rate for the as-ECAPed 5083 Al alloy (route B_c, 473 K) tested at 548 K.

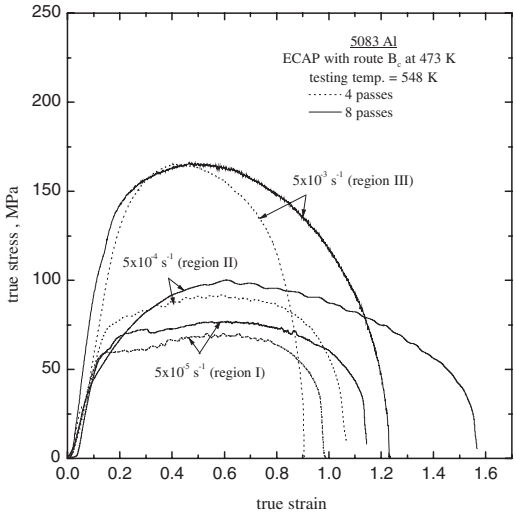

Fig. 5 The true stress-true strain curves for the as-ECAPed 5083 Al alloy (route B_c, 473 K) tested at the strain rates representing each deformation region and at 548 K.

was ~0.1 at low (Region I, $\dot{\varepsilon} < 3 \times 10^{-4}\,s^{-1}$) and high strain rates (Region III, $2 \times 10^{-3}\,s^{-1} < \dot{\varepsilon}$). At the narrow intermediate strain rate region of one order of magnitude (Region II, $3 \times 10^{-4}\,s^{-1} < \dot{\varepsilon} < 2 \times 10^{-3}\,s^{-1}$), m was about 0.4, indicating potential for superplasticity.

Elongation to failure (e_f) of both samples was plotted as a function of the initial strain rate in Fig. 4. After 4 passes, e_f was in the range of 120~150% and seemed to be independent of the strain rate except a slight decrease at the high strain rates faster than $2 \times 10^{-3}\,s^{-1}$. The variation of e_f of the sample after 8 passes with the strain rate was well matched with that of m in Fig. 3(b). At low (Region I, $m = 0.1$) and high (Region III, $m = 0.1$) strain rates, e_f was less than 200% but the superplastic elongation over ~250% was obtained at intermediate strain rates (Region II, $m = 0.4$). A maximum elongation of 315% was obtained at $5 \times 10^{-4}\,s^{-1}$.

The true stress-true strain curves representing each deformation region of the sample after 8 passes were compared to those of the sample after 4 passes at the identical strain rates in Fig. 5: hereafter, although no distinct deformation regions existed in the deformation of the sample after 4 passes, Region I, II and III were referred to the description for its deformation behavior for the purpose of comparison. At $5 \times 10^{-3}\,s^{-1}$ (Region III), both samples exhibited initial rapid strain hardening followed by immediate strain softening without the steady-state flow. However, the strain softening rate of the sample after 8 passes was slower than that of the sample after 4 passes, resulting larger e_f in the former. The initial rapid strain hardening is frequently observed in the strain hardened materials having a high dislocation density,[18] indicating that a severely deformed structure by ECAP was not fully recovered or recrystallized at the high strain rate region. At $5 \times 10^{-4}\,s^{-1}$ (Region II), strain hardening and softening became more gradual in the sample after 8 passes. However, the initial strain hardening in the sample after 4 passes was faster than that after 8 passes. It indicated that the deformation of the sample after 4 passes involved more extensive lattice dislocation activities. The stress-strain curves of both samples at $5 \times 10^{-5}\,s^{-1}$ (Region I) were quite similar, manifested by brief initial strain hardening followed by the steady-state-like flow.

3.3 Deformed microstructure

Figure 6 shows OM microstructures taken from the fractured sample tested at the strain rates representing each deformation region. At $5 \times 10^{-3}\,s^{-1}$ (Region III), no recrys-

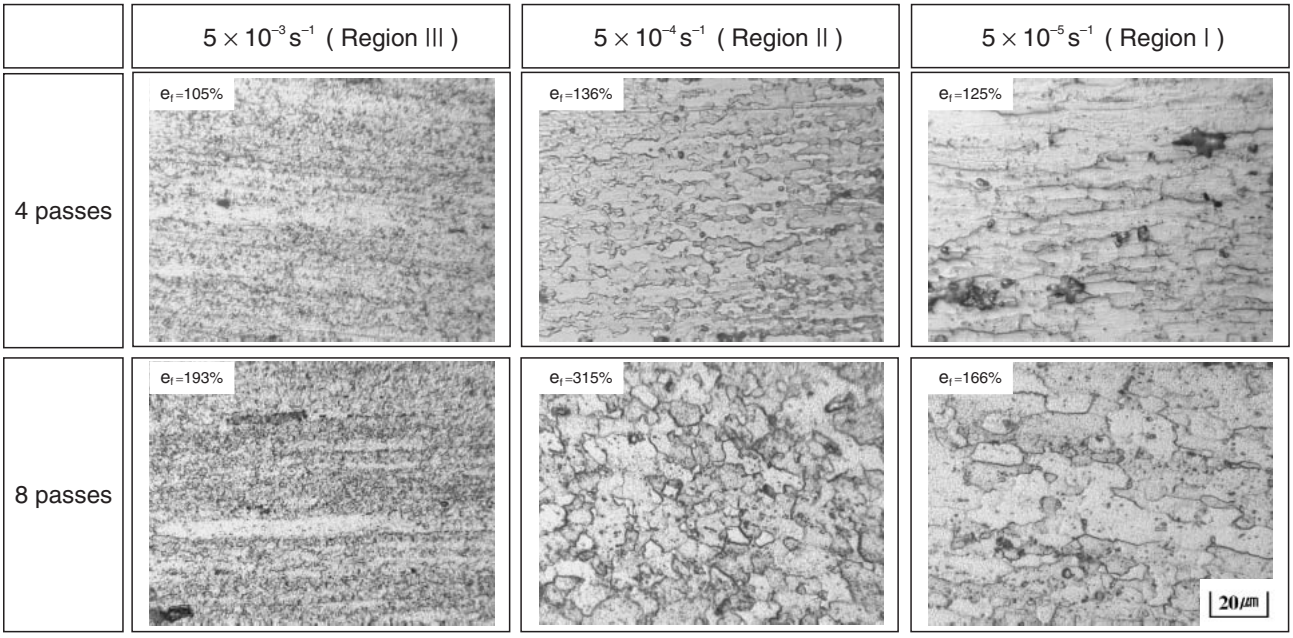

Fig. 6 Optical micrographs of the gage section of the fractured samples of the as-ECAPed 5083 Al alloy (route B_c, 473 K) tested at the strain rates representing each deformation region and at 548 K. The tensile axis is horizontal.

tallization occurred in both cases. It is quite possible that severely strained state induced by ECAP was not fully relaxed at high strain rates, although certain degree of recovery occurred, causing the initial rapid strain hardening as aforementioned in Fig. 5. Quite different recystallized structures were observed at $5 \times 10^{-4}\,s^{-1}$ (Region II). Fine equiaxed recrystallzed grains of $\sim$5 μm dominated the microstructure of the sample after 8 passes. By contrast, the recrystallzed grains of the sample after 4 passes were elongated along the tensile direction. The average linear intercept grain sizes along the transverse and longitudinal directions were $\sim$5 μm and $\sim$13 μm, respectively. At $5 \times 10^{-5}\,s^{-1}$ (Region I), grain elongation in the sample after 4 passes became more extensive with concurrent grain growth: the average linear intercept grain sizes along the transverse and longitudinal directions were $\sim$8 μm and $\sim$20 μm, respectively. In the sample after 8 passes, isotropic dynamic grain growth dominantly occurred and grain elongation was not significant. The above findings along with the mechanical data strongly indicate that deformation of the sample after 4 passes would be governed by a certain form of intragranular dislocation activity causing grain elongation, and LTS of the sample after 8 passes was attributed to grain boundary sliding preserving equiaxed grain shape.

4. Discussion

4.1 Deformation behavior

As discussed in the preceding section, the deformation characteristics and the resultant grain morphology of the samples after 4 and 8 passes were quite different, indicating operation of different deformation mechanisms. Considering the identical experimental conditions and the similar grain size, it is quite probable that these differences resulted primarily from the difference of the initial boundary characteristics. In order to achieve superplasticity, high angle boundaries are required for easy grain boundary sliding. In the present case, a portion of high angle boundaries in the sample after 4 passes was much lower than that in the sample after 8 passes. Komura *et al.*[13] reported that a short period of static annealing, *i.e.* a holding duration of the sample at the testing temperature to reach thermal equilibrium prior to deformation, was not sufficient for the conversion of low angle boundaries to high angle boundaries. In addition, Nieh *et al.*[19] pointed out that continuous recrystallization during high strain rate superplasticity of the cold rolled Al-6Mg-0.3Sc, where the testing temperature was much higher than that in the present case, was not accomplished at the initial stage of deformation, *i.e.* an elongation up to $\sim$100%. Therefore, it is anticipated that a considerable portion of low angle boundaries remained at the initial stage of deformation in the sample after 4 passes. Consequently, grain boundary sliding in the sample after 4 passes would be relatively difficult to occur compared to the sample after 8 passes, and a certain form of lattice dislocation activity could dominate deformation of the former instead of grain boundary sliding. In the next section, the deformation mechanisms of both cases will be examined in light of the standard deformation mechanisms.

4.2 Deformation mechanisms

4.2.1 After 4 passes

Deformation of the sample after 4 passes was characterized by $m = 0.2$ (equivalent to the stress exponent $n = 5$ where $n = 1/m$), $e_f = 120\sim150\%$, and grain elongation. These characteristics are very similar to those of dislocation climb mechanism in the creep of the solid-solution alloys.[20,21] Yavari and Langdon[22] reported that there is a transition of the deformation mechanism from viscous glide to climb in the creep of Al-5 mass %Mg solid-solution alloy at high stresses at which dislocations break away from the solute atmospheres. This possibility is examined here since

the Mg content of the present alloy (4.4 mass %) was comparable to that of the alloy used by Yavari and Langdon.[22)]

The critical stress (σ_b) for this process was given by Friedel[23)] as

$$\sigma_b = \frac{{W_m}^2 c}{5b^3 kT} \tag{1a}$$

$$W_m = -\frac{1}{2\pi}\left(\frac{1+\nu}{1-\nu}\right) G|\Delta V_a| \tag{1b}$$

where W_m is the binding energy between the dislocation and the solute atom, c is the atomic concentration of the solute, b is the Burgers vector, k is the Boltzmann constant and T is the absolute temperature, ν is the Poisson's ratio, G is the shear modulus, and ΔV_a is the atomic volume difference between the solute and solvent atoms. Using eq. (1), a transition of deformation mechanism from viscous glide to climb can be examined by constructing a shear modulus normalized logarithm plot of $({W_m}^2 c/Gb^3 kT)$ *vs* (σ/G). Such a plot is depicted in Fig. 7. In this plot, the inclined line represents the transition condition between viscous glide (left side) and climb (right side) after breakaway. The horizontal line covers the present experimental range of (σ/G) where $\sigma = 71 \sim 199$ MPa. In the calculation, the following values were used:[24)] $\Delta V_a = 5.8 \times 10^{-30}\,\mathrm{m}^3$, $\nu = 0.34$, G (MPa) $= 3.022 \times 10^4 - 16T$, $b = 2.86 \times 10^{-10}$ m, and $c = 0.0486$ (converting 4.4 mass % Mg into the atomic concentration). As seen in Fig. 7, eq. (1) predicted that the transition would occur at $(\sigma/G) = 4.18 \times 10^{-3}$ (or $\sigma = 89.6$ MPa) and so the present experimental range belonged mostly to the climb regime. One of the distinct microstructures developed by dislocation climb is a subgrain formation. Figure 8 shows TEM micrographs of substructures of the samples after 4 passes deformed to failure. At Region III ($\dot{\varepsilon} = 5 \times 10^{-3}\,\mathrm{s}^{-1}$) (Fig. 8a), the microstructure was similar to that of the as-ECAPed state (Fig. 1a) since recrystallization did not occur even after failure in this region as revealed in Fig. 6. The well-developed subgrains (Fig. 8b) were observed in the sample tested at Region II ($\dot{\varepsilon} = 5 \times 10^{-4}\,\mathrm{s}^{-1}$). Figure 8(c) shows the triple junction of subboundaries observed in the sample tested at Region I ($\dot{\varepsilon} = 5 \times 10^{-5}\,\mathrm{s}^{-1}$): the subgrain size in this case was too large to show an entire subgrain

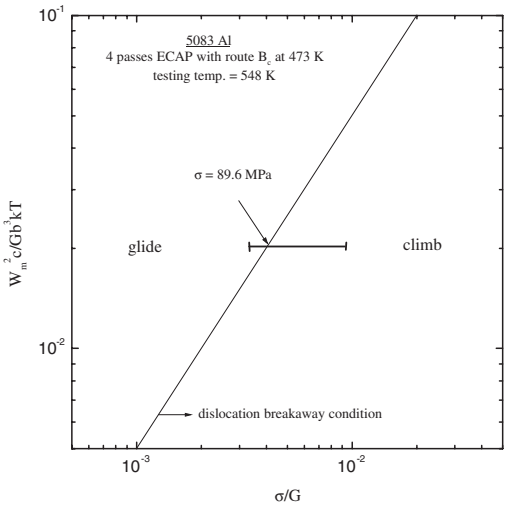

Fig. 7 A plot of $\log({W_m}^2 c/Gb^3 kT)$ *vs* $\log(\sigma/G)$ for a transition between viscous glide and climb associated with dislocation breakaway from solute atmospheres for the sample after 4 passes deformed at 548 K.

under the similar magnification with Figs. 8(a) and (b). The subgrains observed in the sample tested at Regions I and II were not the recovered ones from the initial substructure formed by ECAP. Instead, it is certain that they were developed during deformation by the following justifications; (a) these subgrains were developed inside the fully recrystallized grains (see Fig. 6) and (b) the fact that the subgrain size developed at Region II with higher flow stresses was smaller than that developed at Region I with lower flow stresses agrees, at least qualitatively, with the general finding that the size of subgrains formed by dislocation climb is inversely proportional to the stress.[24)] Figure 8(c) also revealed the long curved dislocation configuration, which is one of the microstructural characteristics induced by viscous glide, at the subgrain interior. This indicates that viscous glide became dominant at relatively low stresses, *i.e.* Region I: the horizontal line in Fig. 7 slightly extends to the glide region. This kind of the feature showing both characteristics of climb (subgrain formation) and viscous glide (long curved dislocations) have been often observed when the deformation mechanism transition occurred.[25)]

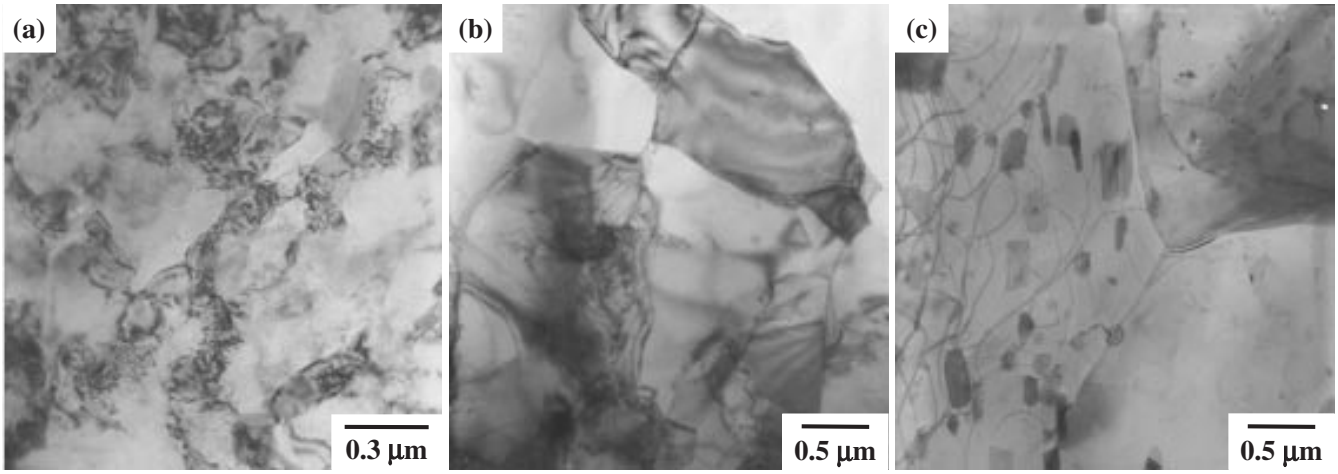

Fig. 8 TEM micrographs showing the substructures developed in the samples after 4 passes deformed to failure. (a) Region III ($\dot{\varepsilon} = 5 \times 10^{-3}\,\mathrm{s}^{-1}$), (b) Region II ($\dot{\varepsilon} = 5 \times 10^{-4}\,\mathrm{s}^{-1}$), (c) Region I ($\dot{\varepsilon} = 5 \times 10^{-5}\,\mathrm{s}^{-1}$).

It is worth mentioning that the possibility of the power law breakdown[20] often observed in the creep of the solid-solution alloys at very high stresses was excluded since the value of m in the present case did not vary with the strain rate while it decreased continuously with increasing the strain rate in the power law breakdown region. The dislocation breakaway model and substructures along with the mechanical data unambiguously informed that dislocation climb governed the deformation of the sample after 4 passes.

4.2.2 After 8 passes

Deformation of the sample after 8 passes was characterized by a sigmoidal behavior in a double logarithmic plot of σ-$\dot{\varepsilon}$, $m = 0.4$ with superplastic elongation in Region II and the equiaxed recrystallized grains. More importantly, as shown in Fig. 6, the recrystallized grain size of the sample deformed in Region II remained as small as $\sim$5 μm even after failure at $\sim$315%. These characteristics clearly demonstrated that LTS of the sample after 8 passes was attributed to grain boundary sliding. More detailed systematic analysis on the LTS behavior of the sample after 8 passes including the deformation behavior at Region I and III was described in Ref. 5) by the present authors.

The experimental range of (σ/G) for the sample after 8 passes, where $\sigma = 73\sim166$ MPa, belonged to the clime regime in Fig. 7: the horizontal line for the sample after 8 passes was not shown due to the overlapping with that of the sample after 4 passes. Nevertheless, grain boundary sliding became a dominant deformation mechanism over dislocation climb in this sample. This can be justified by the facts that (a) the initial microstructural state of the sample after 8 passes, *i.e.* the ultrafine grains and a relatively large portion of high angle boundaries, was preferable for occurrence of grain boundary sliding rather than dislocation creep, and (b) grain boundary sliding and dislocation creep (whether glide or climb) are the independent processes such that a faster process governs overall deformation kinetics.

5. Summary

(1) In the present investigation, the deformation behavior of the UFG 5083 Al alloy prepared by different ECAP passes of 4 and 8 (equivalent effective strains of $\sim$4 or $\sim$8) with route B_c was compared in order to examine the deformation mechanisms operating at low temperature superplastic temperature of 548 K for each case.

(2) The microstructures of the samples after 4 passes and 8 passes exhibited the similar features including the apparent (sub)grain size of $\sim$0.3 μm, ill-defined (sub)-grain boundaries and very high dislocation density etc. However, a portion of boundaries with misorientation in the range of $20^\circ\sim40^\circ$ increased considerably by increasing the ECAP pass. In addition, a portion of high angle boundaries having misorientation angle larger than 15° increased from $\sim$35% after 4 passes to $\sim$50% after 8 passes.

(3) Deformation of the sample after 4 passes was characterized by (a) $m = 0.2$ and $e_f = 120\sim150\%$ at all strain rates, and (b) grain elongation. An examination of the dislocation breakaway model prediction, the mechanical data, and microstructures revealed that dislocation climb was likely to govern the deformation of the sample after 4 passes.

(4) Deformation of the sample after 8 passes was characterized by (a) a sigmoidal behavior in a double logarithmic plot of the stress-strain rate curve, (b) $m = 0.4$ with superplastic elongation at Region II, and (c) the equiaxed recrystallized grains. These characteristics demonstrated that LTS of the sample after 8 passes was attributed to grain boundary sliding.

Acknowledgments

This work was supported by Ministry of Science and Technology of Korea through 'The 21st Century New Frontier Research and Development Program' and 'National Research Laboratory Program'.

REFERENCES

1) M. Mabuchi, H. Iwasaki, K. Yanase and K. Higashi: Scr. Mater. **36** (1997) 681–686.
2) M. Mabuchi, K. Ameyama, H. Iwasaki and K. Higashi: Acta Mater. **47** (1999) 2047–2057.
3) N. Tsuji, K. Shiotsuki, H. Utsunomiya and Y. Saito: Mater. Sci. Forum **304–308** (1999) 73–78.
4) N. Tsuji, K. Shiotsuki and Y. Saito: Mater. Trans., JIM **40** (1999) 765–771.
5) S. Y. Chang, J. G. Lee, K.-T. Park and D. H. Shin: Mater. Trans. **42** (2001) 1074–1080.
6) K. Neishi, T. Uchida, A. Yamaguchi, K. Nakayama, Z. Horita and T. G. Langdon: Mater. Sci. Eng. **A307** (2001) 23–28.
7) K.-T. Park, D. Y. Hwang, S. Y. Chang and D. H. Shin: Metall. Mater. Trans. A **33A** (2002) 2859–2867.
8) L. Dupuy and J.-J. Brandin: Acta Mater. **50** (2002) 3251–3264.
9) J. C. Huang, I. C. Hsiao, T. D. Wang and B. Y. Lou: Scr. Mater. **43** (2000) 213–220.
10) T. R. McNelley, D. L. Swisher, Z. Horita and T. G. Langdon: in '*Ultrafine Grained Materials II*', ed. by Y. T. Zhu, T. G. Langdon, R. S. Mishra, S. L. Semiatin, M. J. Saran and T. C. Lowe, (TMS, Warrendale USA, 2000) 15–24.
11) S. D. Terhune, D. L. Swisher, K. Oh-Ishi, Z. Horita, T. G. Langdon and T. R. McNelley: Metall. Mater. Trans. A **33A** (2002) 2173–2184.
12) P. A. Apps, J. R. Brown, P. B. Prangnell: Acta Mater. **51** (2003) 2811–2822.
13) S. Komura, M. Furukawa, Z. Horita, M. Nemoto and T. G. Langdon: Mater. Sci. Eng. **A297** (2001) 111–118.
14) K. Oh-Ishi, Z. Horita, M. Furukawa, M. Nemoto and T. G. Langdon: Metall. Mater. Trans. A **29A** (1998) 2011–2013.
15) D. H. Shin, B. C. Kim, Y. S. Kim and K.-T. Park: Acta Mater. **48** (2000) 2247–2255.
16) D. H. Shin, J.-J. Park, Y. K. Kim, K.-T. Park and Y. S. Kim: Mater. Sci. Eng. **A323** (2002) 409–415.
17) M. Furukawa, Y. Iwahashi, Z. Horita, M. Nemoto and T. G. Langdon: Mater. Sci. Eng. **A257** (1998) 328–332.
18) Z. Horita, T. Fujinami, M. Nemoto and T. G. Langdon: Metall. Mater. Trans. A **31A** (2000) 691–701.
19) T. G. Nieh, L. M. Hsiung, J. Wadsworth and R. Kaibyshev: Acta Mater. **46** (1998) 2789–2800.
20) O. D. Sherby and P. M. Burke: Prog. Mater. Sci. **13** (1967) 325–390.
21) F. A. Mohamed and T. G. Langdon: Acta Metall. **22** (1974) 779–788.
22) P. Yavari and T. G. Langdon: Acta Metall. **30** (1982) 2181–2196.
23) J. Friedel: in '*Dislocations*', (Pergamon Press, Oxford (UK), 1964) 351–367.
24) J. E. Bird, A. K. Mukherjee ans J. E. Dorn: in '*Quantitative Relation between Properties and Microstructures*', ed. By D. G. Brandon and A. Rosen, (Israel University Press (Jerusalem), 1969) 255.
25) K.-T. Park, E. J. Lavernia and F. A. Mohamed: Acta Metall. Mater. **38** (1990) 1837–1848.